

Local and distant response to intratumoral immunotherapy assessed by immunoPET in mice

Louis Meyblum,^{1,2} Céline Chevalerey,¹ Sandrine Susini,^{3,4} Benoit Jego,¹ Frederic Deschamps,^{2,4} Dimitri Kereselidze,¹ Baptiste Bonnet,^{2,4} Aurelien Marabelle ,^{3,4,5,6} Thierry de Baere,^{2,4,6} Vincent Lebon,¹ Lambros Tselikas ,^{2,3,4,6} Charles Truillet ¹

To cite: Meyblum L, Chevalerey C, Susini S, et al. Local and distant response to intratumoral immunotherapy assessed by immunoPET in mice. *Journal for ImmunoTherapy of Cancer* 2023;**11**:e007433. doi:10.1136/jitc-2023-007433

► Additional supplemental material is published online only. To view, please visit the journal online (<http://dx.doi.org/10.1136/jitc-2023-007433>).

LM and CC contributed equally.

LM and CC are joint first authors.

Accepted 12 October 2023



© Author(s) (or their employer(s)) 2023. Re-use permitted under CC BY-NC. No commercial re-use. See rights and permissions. Published by BMJ.

For numbered affiliations see end of article.

Correspondence to

Dr Charles Truillet; charles.truillet@universite-paris-saclay.fr

ABSTRACT

Background Despite the promising efficacy of immune checkpoint blockers (ICB), tumor resistance and immune-related adverse events hinder their success in cancer treatment. To address these challenges, intratumoral delivery of immunotherapies has emerged as a potential solution, aiming to mitigate side effects through reduced systemic exposure while increasing effectiveness by enhancing local bioavailability. However, a comprehensive understanding of the local and systemic distribution of ICBs following intratumoral administration, as well as their impact on distant tumors, remains crucial for optimizing their therapeutic potential.

To comprehensively investigate the distribution patterns following the intratumoral and intravenous administration of radiolabeled anti-cytotoxic T-lymphocyte-associated protein 4 (CTLA-4) and to assess its corresponding efficacy in both injected and non-injected tumors, we conducted an immunoPET imaging study.

Methods CT26 and MC38 syngeneic colorectal tumor cells were implanted subcutaneously on both flanks of Balb/c and C57Bl/6 mice, respectively. Hamster anti-mouse CTLA-4 antibody (9H10) labeled with zirconium-89 (⁸⁹Zr]9H10) was intratumorally or intravenously administered. Whole-body distribution of the antibody was monitored by immunoPET imaging (n=12 CT26 Balb/c mice, n=10 MC38 C57Bl/6 mice). Tumor responses to injected doses (1–10 mg/kg) were correlated with specific uptake of [⁸⁹Zr]9H10 (n=24). Impacts on the tumor microenvironment were assessed by immunofluorescence and flow cytometry.

Results Half of the dose was cleared into the blood 1 hour after intratumoral administration. Despite this, 7 days post-injection, 6–8% of the dose remained in the intratumoral-injected tumors. CT26 tumors with prolonged ICB exposure demonstrated complete responses. Seven days post-injection, the contralateral non-injected tumor uptake of the ICB was comparable to the one achieved through intravenous administration (7.5±1.7% ID.cm⁻³ and 7.6±2.1% ID.cm⁻³, respectively) at the same dose in the CT26 model. This observation was confirmed in the MC38 model. Consistent intratumoral pharmacodynamic effects were observed in both intratumoral and intravenous treatment groups, as evidenced by a notable increase in CD8+T cells within the CT26 tumors following treatment.

WHAT IS ALREADY KNOWN ON THIS TOPIC

⇒ Immune-related adverse events greatly hinder the efficacy of immune checkpoint blockers, particularly anti-cytotoxic T-lymphocyte-associated protein 4 (CTLA-4) antibodies. However, the local delivery of anti-CTLA-4 shows promise in mitigating these events, necessitating further research for a comprehensive understanding.

WHAT THIS STUDY ADDS

⇒ ImmunoPET monitoring of radiolabeled anti-CTLA-4 demonstrates superior local drug bioavailability with intratumoral antibody injection, lower systemic exposure in healthy tissues with equivalent accumulation, and efficacy in distant non-injected tumors versus intravenously-treated mice.

HOW THIS STUDY MIGHT AFFECT RESEARCH, PRACTICE OR POLICY

⇒ Our findings highlight the importance of immunoPET imaging and pharmacokinetic modeling as valuable tools for enhancing interventional radiology for local tumorous injection commonly used in clinical protocols and offering a potent predictive biomarker.

Conclusions ImmunoPET-derived pharmacokinetics supports intratumoral injection of ICBs to decrease systemic exposure while maintaining efficacy compared with intravenous. Intratumoral-ICBs lead to high local drug exposure while maintaining significant therapeutic exposure in non-injected tumors. This immunoPET approach is applicable for clinical practice to support evidence-based drug development.

BACKGROUND

With the growing landscape of tumor immune regulation, immunotherapy, particularly immune-checkpoint blockers (ICBs) such as anti-cytotoxic T-lymphocyte-associated protein 4 (CTLA-4), based on a monoclonal antibody scaffold, hold a forefront position in cancer management.¹ Despite remarkably durable responses, resistance to ICBs

dampens their impact. This has been linked to several factors, including tumor microenvironment alterations, which can be bypassed notably by combination with other ICBs.² Clinical trials have demonstrated high synergistic benefits with systemic ICB combinations.^{3,4} However, such combinations are not without challenges since immune-related adverse events can limit their success.^{5–7} The high plasma bolus associated with intravenous administration results in a much higher peak concentration, particularly in the liver, heart, and colon.^{8,9} Local delivery offers a potent means of overcoming these adverse events while inducing durable responses. Intratumoral (IT) injection relies on the direct delivery of ICBs into the tumor, a straightforward concept that requires adequate technical background.¹⁰ The number of clinical trials addressing IT injection has burgeoned in the last 10 years.¹¹

Several questions must be addressed when developing IT clinical trials. Limiting factors include ICB pharmacokinetics, whole-tissue distribution over time, and defining several tumor microenvironment factors such as the homing of T cells, local regulatory T cells (Treg), and macrophages. In addition, distant effects on non-injected tumor sites are limited,¹² and the challenge is understanding if this is due to an insufficient drug dose or insufficient cytotoxic immune infiltration. IT immunotherapy efficacy is driven by drug distribution kinetics within the injected (enestic) tumor and distant (anesthetic) tumor.¹³

Despite their importance, whole-body pharmacokinetic studies for injection techniques are lacking.¹⁴ ImmunoPET presents the advantage of revealing distribution over time of radiolabeled ICBs at the molecular level, as demonstrated by Momin *et al* in vivo, with the retention of interleukin-2 in the enestic tumor.¹⁵ The pharmacokinetic analyses based on positron emission tomography (PET) imaging revealed that maximal tumor exposure was correlated to an efficient tumorous response. For other ICBs, redistribution via blood circulation for anesthetic responses in distant tumors has yet to be elucidated. IT delivery of anti-CTLA-4 is of particular interest given its high systemic toxicity.¹⁶ This ICB has been evaluated in multiple mouse models with impressive therapeutic responses,^{17–19} but none have evaluated anesthetic tumors in terms of accurate dose evaluation. This study proposes a holistic approach evaluating the kinetic distribution of IT-injected anti-CTLA-4 in enestic and anesthetic tumors, using pharmacokinetic modeling from immunoPET with the radionuclide isotope zirconium 89 (⁸⁹Zr; 3.3 days half-life).

METHODS

Radiolabeling of 9H10 and its isotype with [⁸⁹Zr]

9H10 is a hamster antibody directed against the mouse CTLA-4 from Bio X Cell (Catalog #BE0131). Its isotype recommended by Bio X Cell is the polyclonal Syrian Hamster IgG (Bio X Cell Catalog#BE0087). 9H10 and its isotype were covalently conjugated with the chelator p-isothiocyanatobenzyl-desferrioxamine

(p-NCS-Bz-DFO, Macrocyclics) on random lysine residues. Radiolabeling with ⁸⁹Zr (PerkinElmer) was performed according to a published protocol.^{20,21} Briefly 1 mL of 9H10 solution (5 mg/mL in phosphate-buffered saline (PBS), pH 9.3) reacted with a fivefold molar excess of p-NCS-Bz-DFO (10 mM in dimethyl sulfoxide (DMSO)) for 45 min at 37°C. The DFO-9H10 and DFO-isotype conjugates were purified with a desalting column (PD-10, GE HealthCare), using PBS as the mobile phase. 150 µL of [⁸⁹Zr]Zr-oxalic acid solution was neutralized with Na₂CO₃ and incubated with DFO-9H10 and DFO-isotype solutions (2.5 mg/mL and 6.4 mg/mL, respectively) for 1 hour at 37°C. The mixtures were adjusted to pH 7.2 with 4-(2-hydroxyethyl)-1-piperazineethanesulfonic acid (HEPES, 1 M, pH 7.1–7.3). The ⁸⁹Zr-labeled DFO-9H10 and the ⁸⁹Zr-labeled DFO-isotype conjugates were first purified with a PD-10 column using PBS as the mobile phase before being further concentrated with a Vivaspin centrifugal concentrator (Sartorius). The radiochemical purity of the ⁸⁹Zr-DFO-9H10 solution was assessed by instant thin-layer chromatography (iTLC) and size-exclusion high-performance liquid chromatography. ⁸⁹Zr-DFO-isotype radiolabeling purity was assessed by iTLC. Binding assays were conducted to assess the minimal influence of the radiolabeling process on the 9H10 antibody's recognition of CTLA-4 (online supplemental figure S5).

Cell culture

The mouse colorectal carcinoma cells lines CT26 (ATCC CRL-2638) and MC38 (Kerafast, ENH204-FP) were cultured in cell culture media such as respectively RPMI-1640 and DMEM medium supplemented with 10% fetal bovine serum (Gibco) and 1% antibiotic-antimycotic solution (Gibco), at 37°C in a humidified atmosphere with 5% CO₂.

Animals and ethics

Animal experiments were performed according to the European Directive 2010/63/EU and its application in French law (Decree No. 2013–118). Research was approved by a local ethics committee (APAFIS #34522–2022010412087915 v1).

CT26 and MC38 tumor cells were collected and suspended at a concentration of 1.10⁶ cells/100 µL in PBS at 4°C. Female Balb/c mice (Janvier Laboratories) and female C57BL/6 mice (Janvier Laboratories) were, respectively, subcutaneously inoculated in both lower flanks with 1×10⁶ CT26 cells and MC38 cells per flank and monitored for 8 days until treatment.

Mice were examined daily and weighed every 2 days. Tumors were measured twice weekly using Vevo F2 ultrasonography system (Fujifilm VisualSonics, Canada). Each tumor was measured in the three planes of space with a high-frequency linear transducer (20–46 MHz), allowing calculation of the tumor volume.

[⁸⁹Zr]9H10/9H10 and [⁸⁹Zr]Isotype imaging

Mice were allocated to two experimental groups evaluating (1) the pharmacokinetic and biodistribution of anti-CTLA-4 with [⁸⁹Zr]9H10 and [⁸⁹Zr]Isotype immunoPET imaging and (2) antitumoral efficacy in relation to [⁸⁹Zr]9H10 immunoPET tumorous distribution (online supplemental figure S1 and table S1). Twelve mice (age 10±1 weeks; 18.1±0.9g) were used for the pharmacokinetic/biodistribution experiment for the CT26 model and 10 mice (age 10±1 weeks; 19.7±1.0g) for the MC38 model. Intravenous administration (100µg, 4.8±0.2MBq; n=6 for CT26 and 100µg, 2.3±0.3n=5 for the MC38) was compared with IT injection in one flank (enestic tumor; 100µg for 10µL, 4.6±0.6MBq; n=6 for the CT26 and 100µg for 10µL, 2.1±0.3MBq n=5 for MC38) (online supplemental figure S2). For the pharmacokinetic and biodistribution of the isotype group, nine mice (age 10 weeks, 20.6±1.5g) were injected with 100µg of [⁸⁹Zr] Isotype: four intratumorally and five intravenously (with 1.2±0.1MBq for the IT and 1.5±0.3MBq for the intravenous group, respectively). In the antitumoral efficacy experiment, 24 mice (age 10±1 weeks; 19.2±1.1g) bearing CT26 model were divided into four groups: (1) control, with IT injection of a polyclonal Syrian Hamster IgG without PET imaging (100±9.8µg/10µL), (2) 20µg IT injection (1mg/kg) with [⁸⁹Zr]9H10 at 3.7±0.1 MBq/10µL, (3) 100µg IT injection (5mg/kg) with [⁸⁹Zr]9H10 at 3.7±0.1 MBq/10µL, and (4) 200µg IT injection (10mg/kg) with [⁸⁹Zr]9H10 at 3.6±0.3 MBq/10µL (online supplemental figure S3). [⁸⁹Zr]9H10 solutions were concentrated to 10µL per dose to avoid exceeding 10% of the tumor volume. After treatment, tumors were measured twice weekly for 4 weeks using an ultrasonography system (FUJIFILM VisualSonics, online supplemental figure S4).

PET emission scans were performed using microPET scanners (Siemens). PET images were reconstructed with the maximum a posteriori algorithm (OP-OSEM3D-MAP) (2 OSEM3D iterations, 18 MAP iterations with 16 MAP subsets). This iterative deconvolution algorithm enhanced the spatial resolution, achieved throughout the entire field of view, devoid of directional discrepancies. A 60min dynamic PET scan was performed immediately after the injection of the [⁸⁹Zr]9H10. Twenty min static PET scans were subsequently acquired at selected times (4, 24, 48, 72 hours, and 7days) post-injection. Volumes of interest (VOIs) were defined with PMOD software (V.3.9). Fixed-size spherical VOIs (3.5–8mm³) were drawn in representative parts of the brain, heart, liver, spleen, inguinal lymph nodes, kidney, intestines, bone, and muscle. Subcutaneous tumors were delineated semi-automatically. The mean activity concentration (kBq.cm⁻³) in each VOI was divided by the total injected dose (kBq) to obtain the percentage of injected dose per volume of tissue (%ID.cm⁻³).

Ex vivo biodistribution

Immediately after the last PET imaging session, mice were sacrificed by cervical dislocation. Blood and major organs (brain, heart, lung, liver, kidney, spleen, intestine, muscle, and bone) were collected, weighed, and counted with

a Wizard² gamma counter (PerkinElmer). Radioactivity data (kBq) were background-corrected, decay-corrected to injection time, and divided by the total injected activity (kBq) and the organ weight (g), to obtain the percentage injected dose per gram of tissue (%ID/g) (online supplemental figure S6).

Pharmacokinetic modeling

Plasma activity concentrations were calculated from image-derived whole-blood activity concentrations from the left cardiac ventricle within the CT26 model. Areas under the curve (AUC) of the intravenous and IT groups were compared with obtain the bioavailable fraction (F). The measured signal in tissue is the sum of the specific uptake due to the target engagement by the radiolabeled antibody and the non-specific uptake from activity in blood and interstitial fluid, especially in tumors benefiting from the enhanced permeation effect. These two components can be isolated by Patlak linearization.²² The slope represents the net rate of irreversible uptake, Ki (in mL.g⁻¹.min⁻¹), and the offset represents the distribution volume, V_T (in mL.cm⁻³). The reversible and irreversible contributions to the uptake of [⁸⁹Zr]9H10 at the different time points were calculated as described by Jauw *et al.*²³

Immunofluorescence and autoradiography

For the pharmacokinetic/biodistribution experiment, after the last imaging session at 7 days, tumors of each group, control, intravenous, and IT (enestic and anenestic), were collected. Excised tumors were snap-frozen and stored at -80°C until processing. Frozen tumors were cryosectioned as 10µm thick slices. Frozen tumor sections were fixed for 10min at room temperature in 10% neutral-buffered formalin solution (Sigma-Aldrich). Non-specific binding sites were blocked by incubation for 2 hours at room temperature with 10% fetal bovine serum (Gibco) and 1% bovine serum albumin (Thermo Fisher). After blocking, treated tumor slides were incubated overnight at 4°C with goat anti-hamster secondary antibody conjugated with Alexa Fluor 546 (Thermo Fisher), to target the 9H10 antibody structure. DAPI (4',6-diamidino-2-phenylindole) was used for nuclear acid staining in fluorescence microscopy. Transmitted light images of stained tumor sections were acquired with the Axio Observer 5 microscope (Zeiss) at 20× magnification. Image post-processing (stitching, white balance, global contrast adjustment and addition of scale bar) was performed with ZEN software (V.2.6, Zeiss). To determine [⁸⁹Zr]9H10 distribution within the tumor precisely, tissue sections (10µm) were exposed to a phosphoscreen for autoradiography and read with a phosphor-imager (GE-Lifesciences, Storm 860).

Flow cytometry

After harvesting the CT26 cells with a GentleMACS dissociator (Miltenyi Biotec), a total of 1×10⁶ cells in 100µL of Cell Staining Buffer (Miltenyi, France). Cells were incubated first at room temperature with the LIVE/DEAD

near-infrared(NIR) fixable viability dye (Invitrogen, France) for 30 min. The Live/Dead was then neutralized with an excess of Cell Staining Buffer. After washing, the cells were centrifuged and resuspended into 100 μ L of Cell Staining Buffer. First, the extracellular proteins were stained with the anti-CD3, anti-CD4, anti-CD8 and anti-CD25 or their corresponding isotype on ice (4°C) for 40 min, then washed and resuspended in 250 μ L of Cell Staining Buffer. The cells were then permeabilized with 250 μ L of Inside Stain Kit (Miltenyi, France) at room temperature for 20 min. Cells were washed and resuspended in 1 mL of the Inside Perm solution (Miltenyi, France). After another washing step, the cells were resuspended in 100 μ L of Inside Perm Solution with the anti-FoxP3-PE or its isotypes for 10 min at room temperature. After washing, cells were analyzed using the Attune NxT Acoustic Focusing Cytometer (Invitrogen). Fluorescence compensations were performed on the corresponding isotypes (Miltenyi, France). Data were analyzed with FlowJo (V.10.7).

Statistics

Statistical analyses were performed with GraphPad Prism (V.9.0.1) and R (V.4.0.2). Influence of the route of administration and treatment was assessed by analysis of variance followed by pairwise comparison of means with Bonferroni's *p* value adjustment. When only the route of administration was considered, two-tailed Student's *t*-test was used. Results were considered statistically significant for *p* values < 0.05.

RESULTS

PET imaging and biodistribution following intratumoral or intravenous administration

The radiochemical purity of [⁸⁹Zr]9H10 exceeded 95% with a molar activity of 130.5 MBq.nmol⁻¹ (online supplemental figure S5). [⁸⁹Zr]9H10 was injected on day 8 after tumor implantation for the CT26 model ($V_{\text{tumor CT26}} = 97.1 \pm 44.0 \text{ mm}^3$) and on day 10 post implantation for the MC38 model ($V_{\text{tumor MC38}} = 139.2 \pm 60.0 \text{ mm}^3$).

Tissue-associated activity, measured by immunoPET at several time points, allowed evaluation of the biodistribution of [⁸⁹Zr]9H10 in blood, organs of interest, and tumor tissue (enestic and anenestic in the IT group) (figure 1, online supplemental table S2 and figure S6,S12). Comparison of *ex vivo* biodistribution with PET image-derived biodistribution confirms a strong correlation between these measurement methods (Pearson *r*=0.92, *p*<0.001; Online supplemental figure S7,S8).

Immediately after IT injection, high activity can be observed in the enestic tumor, compared with the anenestic tumor in the CT26 model. Within 1 hour post-injection, 42.4% ($\pm 5.3\%$) of the dose remained in the enestic tumor (ie, $630.7 \pm 182.1\% \text{ ID.cm}^{-3}$). The activity in the enestic tumor quickly decreases during the first 24 hours and then reaches a "plateau" with an activity of $109.7 \pm 35.1\% \text{ ID.cm}^{-3}$ at day 7 (figure 1C, online supplemental

figure S9,S10). The activity was notably lower in anenestic tumors of the IT group and tumors of the intravenous group, with equivalent distribution patterns, reaching equivalent activity at day 7 after injection (approximately $7.5\% \text{ ID.cm}^{-3}$). In the intravenous group, tumor activity was similar at all time points, irrespective of the tumor site. The co-staining of FoxP3+cells confirms that the anti-CTLA-4 antibody was bound to its target (online supplemental figure 13). The significant differences in tumor-to-blood ratios between the [⁸⁹Zr]9H10 and its isotype also supports specific fixation of the antibody in tumors whatever the injection route (figure 1D). Similarities can be found between the kinetics of the isotype and the 9H10 antibody. However, the isotype is cleared faster from the enestic tumor leading to a significantly lower remaining concentration at 7 days post-injection; $53.9 \pm 10.9\% \text{ ID.cm}^{-3}$ versus $109.7 \pm 35.1\% \text{ ID.cm}^{-3}$, *p*<0.001 for the isotype and the 9H10, respectively (online supplemental figure S9).

Lymph nodes seem to play a major role in the clearance of the antibody from the enestic tumor. The ipsilateral inguinal lymph nodes show a greater uptake of the [⁸⁹Zr]9H10 antibody than the lymph node draining the anenestic tumors (figure 1A). No discernible differences were observed between the lymph nodes draining anenestic tumors and the ones draining tumors within the intravenously injected group. Biodistribution of [⁸⁹Zr]9H10 revealed significantly lower activity in the plasma compartment 1-hour post-injection in the IT group ($0.49 \pm 0.20\% \text{ ID.cm}^{-3}$) compared with the intravenous group ($27.65 \pm 1.79\% \text{ ID.cm}^{-3}$), *p*<0.001. Activity in all organs of interest was lower in the IT group, especially at early time points, compared with the intravenous group (figure 1B). This resulted in a lower delayed accumulation in the elimination organs, especially the liver, with an activity at day 7 of $17.1 \pm 3.5\% \text{ ID.cm}^{-3}$ for the intravenous group and $11.2 \pm 2.8\% \text{ ID.cm}^{-3}$ for the IT group (*p*=0.01; figure 1B). To further support the findings derived from examining the distribution of the anti-CTLA-4 antibody post IT injection in the CT26 model, we extended our analysis to the MC38 model, another colon cancer model (figure 1E). Notably, within the initial hour, 35.4% ($\pm 4.5\%$) of the administered dose persisted in the enestic tumors. Consistent biodistribution patterns were observed in the mirroring experiments in the CT26 model (online supplemental figure 12).

Immunofluorescence and autoradiography specificity

Analysis of the tumor sections on day 7 post-injection showed an equivalent distribution of residual radioactivity (anti-CTLA-4 labeled) to that of the anti-CTLA-4 antibody detected by immunofluorescence, mostly in the periphery of the CT26 tumors (figure 2). Comparing the IT and the intravenous groups, the quantities of anti-CTLA-4 and level of persistent activity were much higher in enestic tumors ($109.74 \pm 35.12\% \text{ ID.cm}^{-3}$) than anenestic tumors ($7.52 \pm 1.73\% \text{ ID.cm}^{-3}$ – *p*<0.001) and

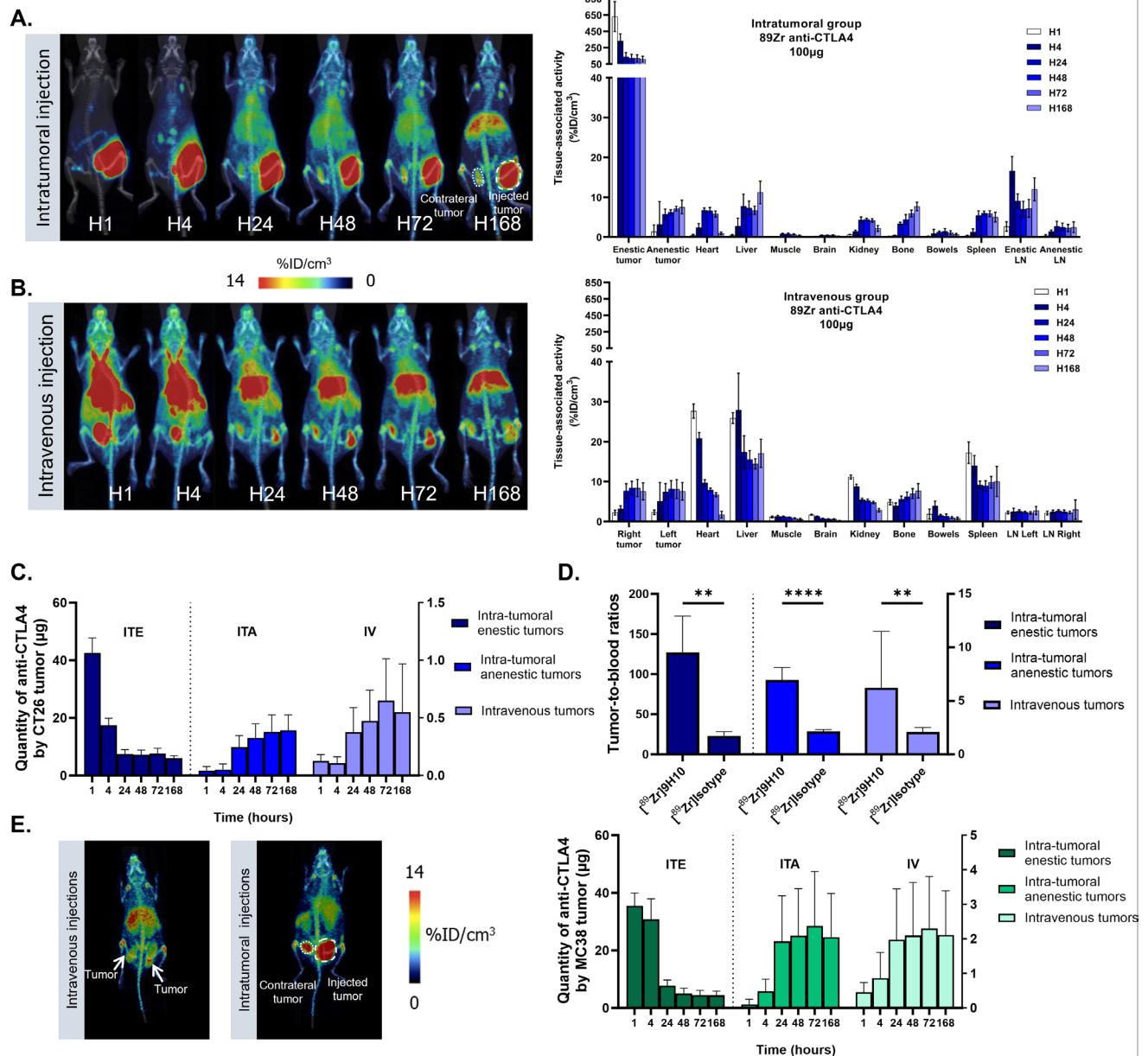


Figure 1 Biodistribution over time of anti-CTLA-4 antibody by PET imaging. (A) Intratumoral injection group and (B) Intravenous injection group representative immunopET maximum intensity projection images of mice bearing a CT26 tumor after administration of [⁸⁹Zr]9H10 (100 µg), over 7 days post-injection and the image-derived in vivo biodistribution of [⁸⁹Zr]9H10. LN=lymph node (inguinal). (C) Quantity of 9H10 in µg of injected antibody in enesthetic (ITE), anesthetic (ITA) and intravenous arm tumors, over 7 days post-injection measured from immunopET imaging-derived biodistribution in CT26 tumor (online supplemental figure S9). (D) Comparison of the tumor-to-blood ratios between the [⁸⁹Zr]isotope and the [⁸⁹Zr]9H10 antibody in the CT26 model at 7 days post-injection. (E) [⁸⁹Zr]9H10 tumor distribution in a MC38 model at 7 days post-injection with representative immunopET maximum intensity projection images of mice bearing a tumor after administration of anti-CTLA-4 radioligand (100 µg) (left). Representation of 9H10 quantity in µg of the ITE, ITA and intravenous (right). Data are presented as mean±SD, n=6 mice/group for the CT26 and n=5/group for the MC38 model for the [⁸⁹Zr]9H10 injection, and n=4 for the intratumoral group and n=5 for the intravenous group for the [⁸⁹Zr]isotope injection in CT26 model, %ID.cm⁻³: percentage injected dose per volume of tissue. CTLA-4, cytotoxic T-lymphocyte-associated protein 4; PET, positron emission tomography; [⁸⁹Zr], zirconium-89.

in the IT group compared with the intravenous group (7.55±2.07 %ID.cm⁻³ – p<0.001).

Pharmacokinetics in the CT26 model

Plasma pharmacokinetic profiles differed between the intravenous and IT groups but resulted in a similar

uptake pattern for intravenous and intratumoral anesthetic tumors at most time points (figure 3A,B). The ratio of plasma AUC between the intravenous and IT groups is 0.70, corresponding to the bioavailable fraction of the IT route. The [⁸⁹Zr]isotope has

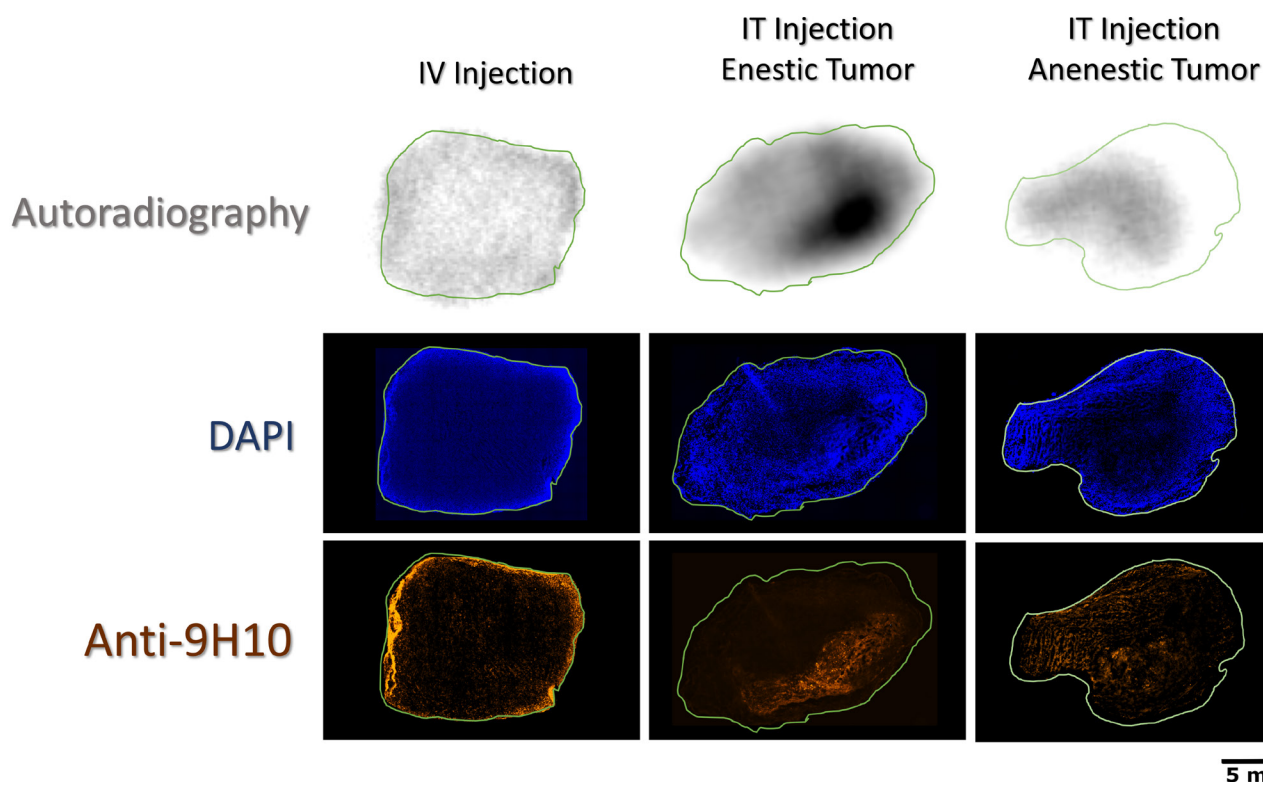


Figure 2 Representative images of tumor sections by immunofluorescence and autoradiography (adjacent slices) showing intratumoral spatial distribution of all cellular nuclei (DAPI), anti-9H10 and persistent radioactivity 7 days post-injection for intratumoral and intravenous administration. Data are presented as mean \pm SD, n=6 mice/group treated at 100 μ g, CT26 model. %ID.cm $^{-3}$: percentage injected dose per volume of tissue. DAPI, 4',6-diamidino-2-phenylindole; IV, intravenous; IT, intratumoral.

an equivalent bioavailable fraction implying that the bioavailability is not driven by the specific fixation of the antibody (online supplemental figure S9).

The reversible and irreversible contributions to the measured activity were comparable in the anenestic tumor in the IT group and the tumors in the intravenous group. The irreversible contribution in the tumor corresponds to the specific target engagement of the anti-CTLA-4 and the reversible contribution corresponds to the non-binding antibody accumulation. Target engagement, irrespective of injection route, was similar. The irreversible and reversible contribution over time allowed identification of the most relevant time point to study the irreversible binding part of the antibody in the IT group, corresponding to the time point 7 days post-injection (figure 3C,D). Using the progressive increase of irreversible contribution to the measured activity, estimated by Patlak linearization, we estimated that 168 hours (ie, 7 days) was the most accurate time point for assessing irreversible binding of the [89 Zr]9H10 antibody to its target in tumor tissue. At earlier time points (notably before 72 hours), measured activity mainly reflected reversible binding corresponding to blood flow. Another reason that can partially explain the major contribution of reversible binding, particularly at the earliest time points, could be the scarcity of target immune cells within the region of interest.

Tumor response in terms of drug administration modality

Antitumoral efficacy was evaluated in terms of [89 Zr]9H10 immunoPET tumorous distribution in the CT26 model. All tumors in the control group (isotype) progressed rapidly, requiring animal sacrifice before the end of the planned follow-up period (figure 4, online supplemental figure S14.). For mice receiving IT anti-CTLA-4 treatment, 17 of the 18 (94%) enestic tumors showed complete response, across all three doses. For anenestic tumors, the complete response rate was 100% (n=6/6) for the 200 μ g group, 83% (n=5/6) for the 100 μ g group, and 50% (n=3/6) for the 20 μ g group. We selected the intermediate dose of 100 μ g to observe the effects of the treatment on T lymphocytes tumor infiltration (online supplemental table S3, gating strategy in online supplemental figure S16). No difference was observed for Treg regulation (CD3 $^{+}$ /CD4 $^{+}$ /CD25 $^{+}$ /FoxP3 $^{+}$) in any group, with all routes of administration of anti-CTLA-4 leading to increased recruitment of CD8 $^{+}$ T lymphocytes in tumors compared with the isotype (figure 4E,F). The infiltration of CD8 $^{+}$ T-lymphocytes was not significantly different between enestic and anenestic tumors 7 days after IT treatment (p=0.94), which aligns well with the observed impact on tumor growth. Moreover, Treg does not seem to be depleted whatever the administration route (IT or intravenous) and the enestic and anenestic tumor (online supplemental table S3). Other immune cell activities may

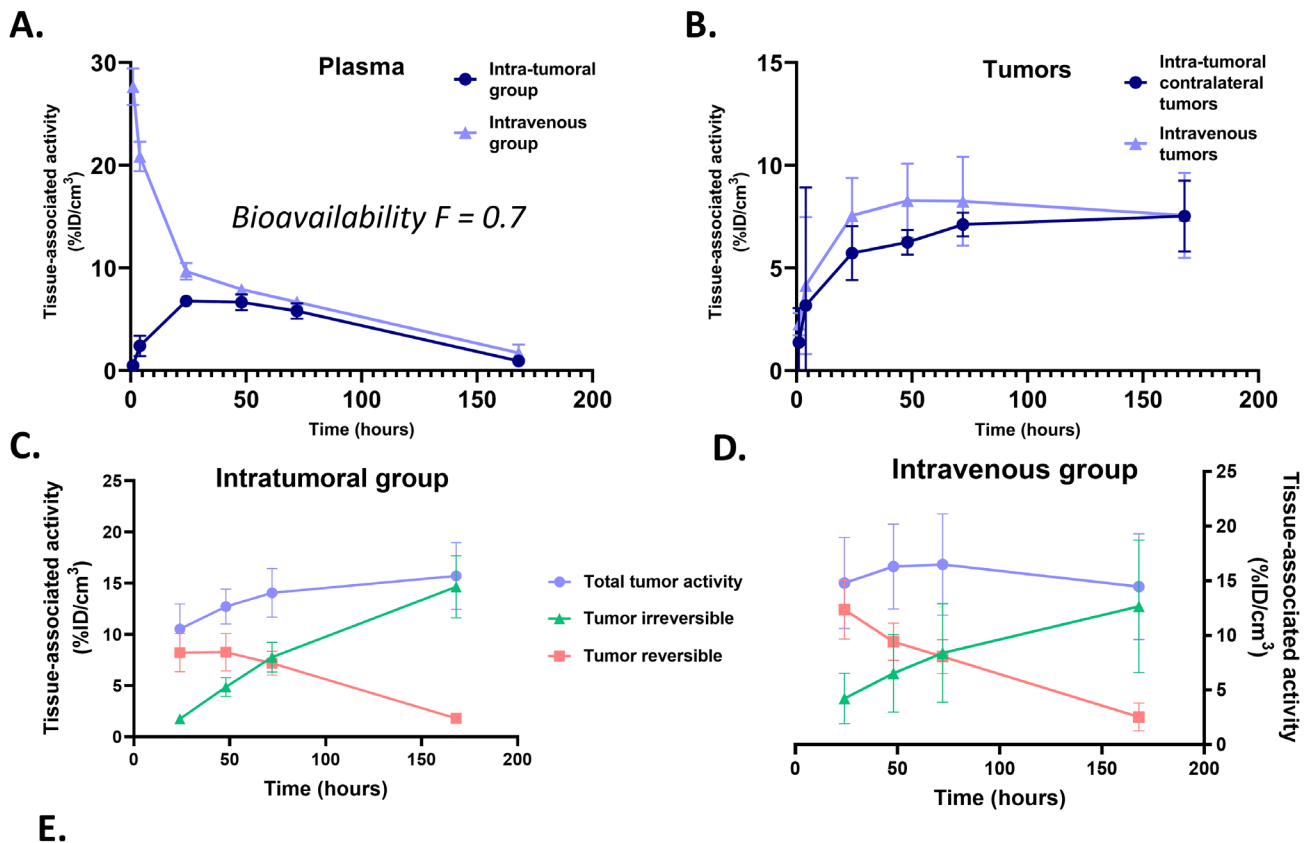


Figure 3 Comparative pharmacokinetic parameters for intravenous and intratumoral injection derived from PET imaging in CT26 model. (A) and (B) ImmunoPET imaging-derived [⁸⁹Zr]9H10 uptake comparison between intravenous and intratumoral groups in plasma (A) and tumors (B) (in anesthetic tumors only for the intratumoral group) over 7 days post-injection. Bioavailability fraction F corresponds to the ratio between intratumoral and intravenous calculated plasma $AUC_{0 \rightarrow \infty}$. (C) and (D) Estimation of reversible and irreversible [⁸⁹Zr]9H10 fixation contributions to measured activity for tumor using Patlak linearization for intratumoral (C) and intravenous (D) groups. (E) Pharmacokinetic parameters for each group for the 100 μg dose (K_i , V_T and AUC) are summarized. Data are presented as mean ± SD, $N=6$ mice/group, %ID.cm⁻³: percentage injected dose per volume of tissue. AUC , area under the curve; PET, positron emission tomography; [⁸⁹Zr], zirconium-89.

play a crucial role in long-term survival and tumor growth and will be further investigated. Given that the time point at 7 days post-injection reliably represents the irreversible fixation of the antibody in the tumor, the amount (in μg) of antibody still present in the tumor could be estimated. These results are summarized in [table 1](#).

DISCUSSION/CONCLUSION

IT-ICBs have shown promise for producing both local and distant effects, but their clinical use is currently limited due to a lack of empirical pharmacokinetic exploration. To address this, we investigated whether anti-CTLA-4

pharmacokinetic data derived from PET imaging could serve as a valuable efficacy biomarker.

In this study, we have shown that ⁸⁹Zr immuno-PET for IT anti-CTLA-4 administration allowed us to establish a precise pharmacokinetic profile of the ICB distribution at various concentrations for both intravenous and IT administration, particularly in the CT26 model. Not surprisingly, around half of the dose was still present in the enestic tumor a few hours post-injection following IT injection. A rapid decrease in the first few days was observed, but a significant proportion of the injected dose (~7%) remained in the tumor 7 days after the IT injection. The concentrations in the enestic tumor at

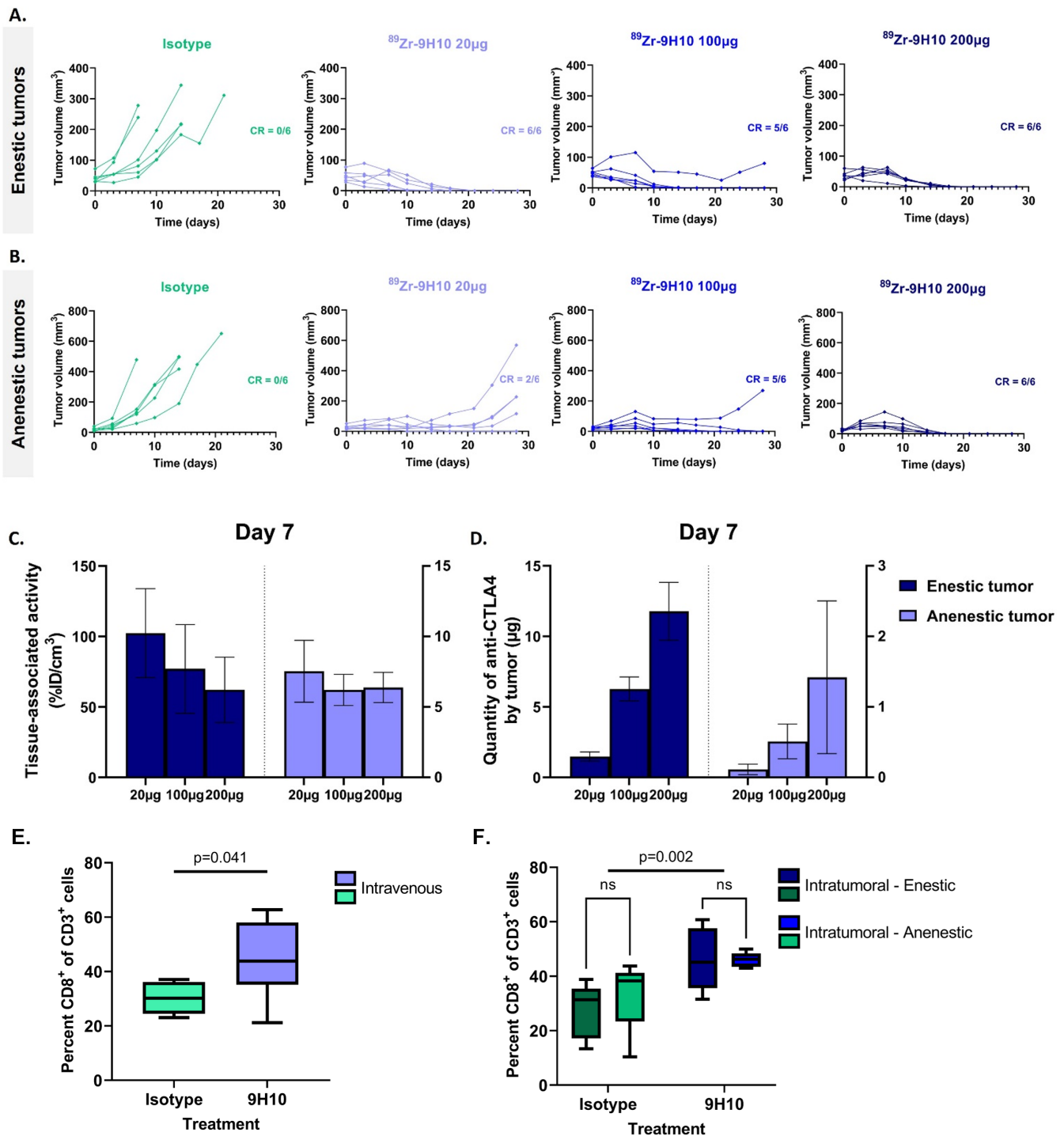


Figure 4 ImmunopET imaging-determined tumor dose and immune checkpoint blocker efficacy with intratumoral injection in CT26 model. (A) and (B) Comparison of tumor volume in the control group and treatment groups following intratumoral injection of an isotype or anti-CTLA-4 (clone 9H10) at three doses: 20 µg (1 mg/kg), 100 µg (5 mg/kg) and 200 µg (10 mg/kg), in enestic tumors (A) and anenestic tumors (B). Tumor evolution data for intravenous injection at 100 µg are presented in online supplemental figure S14. (C) and (D) Tumor distribution of [^{89}Zr]9H10 (C) and dose quantity of 9H10 (D) in enestic and anenestic tumors according to the injected dose. Statistical information on tumor growth impact is represented in online supplemental figure S14. (E) and (F) Tumor infiltration by CD8⁺ T lymphocytes 7 days after intravenous (E) or intratumoral (F) administration of 100 µg anti-CTLA-4 antibody or its isotype. CR, complete response; CTLA, cytotoxic T-lymphocyte-associated protein 4; IT, intratumoral; [^{89}Zr], zirconium-89.

day 7 with IT injection were significantly higher than those achievable intravenously, even with higher intravenous doses (10 mg/kg). The IT route thus offers rapid,

significant, and prolonged exposure of tumor and immune cells to ICB, which could result in significant clinical benefit, as anti-CTLA-4 efficacy has been shown to be

Table 1 [⁸⁹Zr]9H10 quantification in tumor tissue

Treatment group	Injected (enestic) tumor		Contralateral (anenestic) tumor		
	Antibody quantity at day 7 (μg)	Percentage of injected dose	Antibody quantity at day 7 (μg)	Percentage of dose in enestic tumor	Percentage of injected dose
20 μg	1.48 (±0.32)	7.4 (±1.6)	0.11 (±0.07)	7.4 (±4.7)	0.55 (±0.35)
100 μg	6.27 (±0.85)	6.3 (±0.85)	0.51 (±0.25)	8.1 (±4.0)	0.51 (±0.25)
200 μg	11.78 (±2.05)	5.9 (±1.0)	1.42 (±1.11)	12.1 (±9.4)	0.71 (±0.55)

Data are presented as mean±SD.
[⁸⁹Zr], zirconium-89.

dose-dependent.²⁴ The remote tumor distribution profile was confirmed within the second colon cancer model, the MC38 model. Antibody clearance into the lymphatic vessels cannot explain this difference since functional lymphatic vessels are poorly observed in tumors.²⁵ The development of antidrug antibodies that can interfere with ICB release from the tumor, as suggested by Baniel *et al*,²⁶ is unlikely following a single ICB injection. These findings suggest that the tumorous antigen pool was not totally saturated at the lowest dose for the anenestic tumors, as suggested by low tumor content (0.11±0.07 μg at 7 days post-injection). The estimated concentration in the anenestic tumor, ~0.6 nM, was much below anti-CTLA-4's dissociation constant. Compared with intravenous administration, prolonged exposure via IT ensured complete inhibition of the relevant cells, mainly Treg, while sparing healthy tissue.

When we compare the distribution of anti-CTLA-4 with an isotope control, it becomes clear that 9H10 uptake within the tumors it is driven by the specific binding to Treg cells, while the non-specific retention due to the enhanced permeability and retention effect or Fc-binding seems to have a relatively low impact.²⁷

As suggested by Fransen *et al*, lower doses injected via the IT route can provide the same efficacy as higher doses delivered systemically.¹⁸ In our experiments, a complete response of the injected tumor was observed in almost all cases irrespective of the dose used (1–10 mg/kg), in agreement with the expected results, given the steep effect-dose with anti-CTLA-4.²⁸

An interesting aspect of this study is the behavior of anenestic tumors implanted contralateral to the IT-injected tumor, designed to mimic metastases in a syngeneic model integrating the impact of the immune system on the mode of administration. Our findings indicate that the mechanism of action in the distant tumor is intricate and not solely attributed to systemic antitumoral immune system activation. In various preclinical studies, a noteworthy reduction in IT Tregs has been observed^{29,30} which contrasts with our clinical observations, that also differ from those reported by Sharma *et al* in human cancers.³¹ Ongoing inquiries continue to delve into this matter. The Patlak approach was used to determine the target engagement in the anenestic tumors compared with tumors treated intravenously. The irreversible uptake

in the tumor (anenestic and intravenous), that is, the target engagement, increases over time with a clear elimination of non-binding antibodies (reversible phase).²³ This demonstrates potentially valuable immunotherapy release over time from the enestic tumor, equivalent to the intravenous injection, without the potential toxicity induced by the intravenous bolus. Low reversible contribution at 7 days suggests that the uptake for an injected dose of 5 mg/kg observed in the anenestic tumor is exclusively associated with monoclonal antibody specific binding at the latest time point.

As observed by Momin *et al*, the injected tumor largely blocks antibody diffusion into plasma following IT injection.¹⁵ While some antibodies bind to the receptors, the majority can move from the tumor into the blood through convective transport, as observed with subcutaneous injection.³² The equivalent plasma dose for IT or intravenous administration at later time points after injection has a direct impact. For the same injected dose (5 mg/kg) intravenous and IT, 7 days after injection, the same antibody concentration was found in the anenestic tumor in the IT group and the tumors in the intravenous group. The corresponding dose-effect relation for anenestic tumors is particularly mesmerizing. In the anenestic tumor, persistent doses higher than 1 μg, 7 days post-injection was linked to an almost complete response with durable tumor remission. Below this dose, the tumor response to treatment was heterogeneous, with initial partial response, followed by a relapse. Multiple doses might be beneficial, especially if we envision decreasing the doses relative to the intravenous dose. A higher injection dose could overcome the problem of relapse but could, theoretically, induce more toxicity, even though we did not observe any adverse effects at 10 mg/kg in our study. The problematics of the immune-related adverse events (irAEs) emergence is particularly acute with anti-CTLA-4 due to a significant dose effect toxicity,¹⁶ especially when combined with anti-programmed death receptor and its ligand (PD-(L)1) in dual therapy.^{6,33} Thus, the high plasma bolus involved via intravenous results in a much higher maximum concentration, particularly in organs at risk of complications (eg, the colon),^{8,9} as well as a lower accumulation of the antibody in the organs of elimination (eg, the liver and the kidneys). The lower exposure via IT of the organs to the antibody and the expected

decrease of irAEs is a further argument in favor of using this injection route, especially as this route usually allows the use of much lower doses (rather than the order of 1 mg/kg). Using slow-release platforms could also be an interesting approach to increase the antibody reserves in the injected tumor.³⁴

We acknowledge that the selection of the CT26 tumor model is limited to those known to be responsive to checkpoint inhibitors.^{35 36} Our objective was to establish a correlation between monoclonal antibody pharmacokinetics and immunotherapy effectiveness. The next ongoing phase involves assessing this injection method in a clinical trial with patients (NCT04823403).

To conclude, direct IT injection presents both advantages and drawbacks. It remains the most often employed local administration route in clinical protocols to date due to its simplicity and the variety of organs that can be reached with modern guidance tools. We demonstrate consequently that immunoPET imaging and attainable pharmacokinetic modeling are highly valuable to intensify interventional radiology, providing a potent predictive biomarker.

Author affiliations

¹Université Paris-Saclay, CEA, CNRS, INSERM UMR1281, Laboratoire d'Imagerie Biomédicale Multimodale Paris Saclay (BioMaps), Orsay, France

²Département d'Anesthésie, Chirurgie et Interventionnel (DACI), Service de Radiologie Interventionnelle, Gustave Roussy, Villejuif, France

³Laboratoire de Recherche Translationnelle en Immunothérapie (LRTI), INSERM U1015, Villejuif, France

⁴BIOHERIS, Centre d'Investigation Clinique, INSERM U1428, Villejuif, France

⁵Gustave Roussy, Villejuif, France

⁶Université Paris Saclay, Saint Aubin, France

Twitter Lambros Tselikas @LambrosTselikas

Acknowledgements Figures were created with BioRender.com and GraphPad Software.

Contributors LM and CC share co-first authorship, reflecting their equal and significant contributions to this work. LM, CC, LT and CT designed research. LM, CC, SS, BJ, FD, DK, BB, AM, TdB, VL, LT and CT performed research. LM, CC, SS, BJ, DK, LT and CT contributed new reagents/analytical tools. LM, CC, SS, AM, TdB, VL, LT and CT, analyzed data and, LM, CC, SS, FD, BB, AM, TdB, VL, LT and CT wrote the paper. CT is responsible for the overall content as guarantor.

Funding This work was funded by both the LRTI and BioMaps Labs. LM funding was granted by the "Année Recherche Grant" from ARS île de France. This work was performed on an imaging platform member of the France Life Imaging network (grant ANR-11-INBS-0006). The authors acknowledge the financial support from ITMO Cancer of Aviesan (Alliance nationale pour les sciences de la vie et de la santé) on funds administered by Inserm (IM2FUS).

Competing interests None declared.

Patient consent for publication Not applicable.

Ethics approval Not applicable.

Provenance and peer review Not commissioned; externally peer reviewed.

Data availability statement Data are available upon reasonable request. All data relevant to the study are included in the article or uploaded as supplementary information.

Supplemental material This content has been supplied by the author(s). It has not been vetted by BMJ Publishing Group Limited (BMJ) and may not have been peer-reviewed. Any opinions or recommendations discussed are solely those of the author(s) and are not endorsed by BMJ. BMJ disclaims all liability and responsibility arising from any reliance placed on the content. Where the content includes any translated material, BMJ does not warrant the accuracy and reliability

of the translations (including but not limited to local regulations, clinical guidelines, terminology, drug names and drug dosages), and is not responsible for any error and/or omissions arising from translation and adaptation or otherwise.

Open access This is an open access article distributed in accordance with the Creative Commons Attribution Non Commercial (CC BY-NC 4.0) license, which permits others to distribute, remix, adapt, build upon this work non-commercially, and license their derivative works on different terms, provided the original work is properly cited, appropriate credit is given, any changes made indicated, and the use is non-commercial. See <http://creativecommons.org/licenses/by-nc/4.0/>.

ORCID iDs

Aurelien Marabelle <http://orcid.org/0000-0002-5816-3019>

Lambros Tselikas <http://orcid.org/0000-0002-8878-4916>

Charles Truillet <http://orcid.org/0000-0002-1782-5418>

REFERENCES

- Bouleau A, Lebon V, Truillet C. PET imaging of immune Checkpoint proteins in oncology. *Pharmacol Ther* 2021;222:107786.
- Vafaei S, Zekiy AO, Khanamir RA, et al. Combination therapy with immune Checkpoint inhibitors (IcIs); a new frontier. *Cancer Cell Int* 2022;22:2.
- Hellmann MD, Rizvi NA, Goldman JW, et al. Nivolumab plus Ipilimumab as first-line treatment for advanced non-small-cell lung cancer (Checkmate 012): results of an open-label, phase 1, Multicohort study. *Lancet Oncol* 2017;18:31–41.
- Larkin J, Chiarion-Sileni V, Gonzalez R, et al. Five-year survival with combined Nivolumab and Ipilimumab in advanced Melanoma. *N Engl J Med* 2019;381:1535–46.
- Wojtukiewicz MZ, Rek MM, Karpowicz K, et al. Inhibitors of immune checkpoints-PD-1, PD-L1, CTLA-4-new opportunities for cancer patients and a new challenge for internists and general practitioners. *Cancer Metastasis Rev* 2021;40:949–82.
- Larkin J, Chiarion-Sileni V, Gonzalez R, et al. Combined Nivolumab and Ipilimumab or monotherapy in untreated Melanoma. *N Engl J Med* 2015;373:23–34.
- Rotte A. Combination of CTLA-4 and PD-1 blockers for treatment of cancer. *J Exp Clin Cancer Res* 2019;38:255.
- Bertrand A, Kostine M, Barnette T, et al. Immune related adverse events associated with anti-CTLA-4 antibodies: systematic review and meta-analysis. *BMC Med* 2015;13:211.
- Centanni M, Moes D, Trocóniz IF, et al. Clinical pharmacokinetics and pharmacodynamics of immune Checkpoint inhibitors. *Clin Pharmacokinet* 2019;58:835–57.
- Tselikas L, Champiat S, Sheth RA, et al. Interventional Radiology for local Immunotherapy in oncology. *Clin Cancer Res* 2021;27:2698–705.
- Champiat S, Tselikas L, Farhane S, et al. Intratumoral Immunotherapy: from trial design to clinical practice. *Clin Cancer Res* 2021;27:665–79.
- Raman SS, Hecht JR, Chan E. Talimogene Laherparepvec: review of its mechanism of action and clinical efficacy and safety. *Immunotherapy* 2019;11:705–23.
- Marabelle A, Andtbacka R, Harrington K, et al. Starting the fight in the tumor: expert recommendations for the development of human Intratumoral Immunotherapy (HIT-IT). *Ann Oncol* 2018;29:2163–74.
- Panizza BJ, de Souza P, Cooper A, et al. Phase I dose-escalation study to determine the safety, tolerability, preliminary efficacy and pharmacokinetics of an Intratumoral injection of Tigilanol Tiglate (EBC-46). *EBioMedicine* 2019;50:433–41.
- Momin N, Palmeri JR, Lutz EA, et al. Maximizing response to Intratumoral Immunotherapy in mice by tuning local retention. *Nat Commun* 2022;13:109.
- Darnell EP, Mooradian MJ, Baruch EN, et al. Immune-related adverse events (irAEs): diagnosis, management, and clinical pearls. *Curr Oncol Rep* 2020;22:39.
- Simmons AD, Moskalenko M, Creson J, et al. Local secretion of anti-CTLA-4 enhances the therapeutic efficacy of a cancer Immunotherapy with reduced evidence of systemic Autoimmunity. *Cancer Immunol Immunother* 2008;57:1263–70.
- Fransen MF, van der Sluis TC, Ossendorp F, et al. Controlled local delivery of CTLA-4 blocking antibody induces Cd8+ T-cell-dependent tumor eradication and decreases risk of toxic side effects. *Clin Cancer Res* 2013;19:5381–9.
- van Hooren L, Sandin LC, Moskalev I, et al. Local Checkpoint inhibition of CTLA-4 as a monotherapy or in combination with anti-Pd1 prevents the growth of murine bladder cancer. *Eur J Immunol* 2017;47:385–93.

- 20 Bouleau A, Nozach H, Dubois S, *et al.* Optimizing Immuno-PET imaging of tumor PD-L1 expression: pharmacokinetic, Biodistribution, and Dosimetric comparisons of ⁸⁹Zr-labeled anti-PD-L1 antibody formats. *J Nucl Med* 2022;63:1259–65.
- 21 Vosjan M, Perk LR, Visser GWM, *et al.* Conjugation and Radiolabeling of Monoclonal antibodies with Zirconium-89 for PET imaging using the Bifunctional Chelate P-Isothiocyanatobenzyl-Desferrioxamine. *Nat Protoc* 2010;5:739–43.
- 22 Patlak CS, Blasberg RG. Graphical evaluation of blood-to-brain transfer constants from multiple-time uptake data. generalizations. *J Cereb Blood Flow Metab* 1985;5:584–90.
- 23 Jauw YWS, O'Donoghue JA, Zijlstra JM, *et al.* 89Zr-Immuno-PET: toward a noninvasive clinical tool to measure target engagement of therapeutic antibodies in vivo. *J Nucl Med* 2019;60:1825–32.
- 24 Karimi A, Alilou S, Mirzaei HR. Adverse events following administration of anti-Ctla4 antibody Ipilimumab. *Front Oncol* 2021;11:624780.
- 25 Hagendoorn J, Tong R, Fukumura D, *et al.* Onset of abnormal blood and Lymphatic vessel function and interstitial hypertension in early stages of carcinogenesis. *Cancer Res* 2006;66:3360–4.
- 26 Baniel CC, Sumiec EG, Hank JA, *et al.* Intratumoral injection reduces toxicity and antibody-mediated neutralization of Immunocytokine in a mouse Melanoma model. *J Immunother Cancer* 2020;8:e001262.
- 27 Wu J. The enhanced permeability and retention (EPR) effect: the significance of the concept and methods to enhance its application. *J Pers Med* 2021;11:771.
- 28 Ascierto PA, Del Vecchio M, Robert C, *et al.* n.d. Ipilimumab 10 mg/kg versus Ipilimumab 3 mg/kg in patients with Unresectable or metastatic Melanoma. *Lancet Oncol*
- 29 Francis DM, Manspeaker MP, Schudel A, *et al.* Blockade of immune checkpoints in lymph nodes through Locoregional delivery augments cancer Immunotherapy. *Sci Transl Med* 2020;12:eaay3575.
- 30 Shklovskaya E, Pedersen B, Stewart A, *et al.* Durable responses to anti-Pd1 and anti-Ctla4 in a Preclinical model of Melanoma displaying key Immunotherapy response biomarkers. *Cancers (Basel)* 2022;14:4830.
- 31 Sharma A, Subudhi SK, Blando J, *et al.* Anti-CTLA-4 Immunotherapy does not deplete Foxp3⁺ regulatory T cells (Tregs) in human cancers-response. *Clin Cancer Res* 2019;25:3469–70.
- 32 Ryman JT, Meibohm B. Pharmacokinetics of Monoclonal antibodies: pharmacokinetics of Monoclonal antibodies. *CPT Pharmacomet Syst Pharmacol* 2017;6:576–88.
- 33 Rotte A. Combination of CTLA-4 and PD-1 blockers for treatment of cancer. *J Exp Clin Cancer Res* 2019;38:255:255..
- 34 Tselikas L, de Baere T, Isoardo T, *et al.* Pickering emulsions with Ethiodized oil and nanoparticles for slow release of Intratumoral anti-Ctla4 immune Checkpoint antibodies. *J Immunother Cancer* 2020;8:e000579.
- 35 Castle JC, Loewer M, Boegel S, *et al.* Immunomic, Genomic and Transcriptomic characterization of Ct26 colorectal carcinoma. *BMC Genomics* 2014;15:190.
- 36 Selby MJ, Engelhardt JJ, Johnston RJ, *et al.* Preclinical development of Ipilimumab and Nivolumab combination Immunotherapy: Mouse tumor models, in vitro functional studies, and cynomolgus Macaque toxicology. *PLOS ONE* 2016;11:e0167251.